AIP | Journal of Applied Physics

Enhanced magnetization and improved insulating character in Eu substituted BiFeO3

T. Durga Rao[1], R. Ranjith[2] and Saket Asthana[1,a)]

1 Advanced Functional Materials Laboratory, Department of Physics, Indian Institute of Technology Hyderabad, Andhra Pradesh–502205, India
2 Department of Materials Science and Metallurgical Engineering, Indian Institute of Technology Hyderabad, Andhra Pradesh–502205, India

AIP | Journal of Applied Physics 115, 124110 (2014).

http://dx.doi.org/10.1063/1.4869775

Enhanced magnetization and improved insulating character in Eu substituted $BiFeO_3$

T. Durga Rao[1], R. Ranjith[2], Saket Asthana[1*]

[1]*Advanced Functional Materials Laboratory, Department of Physics,*
Indian Institute of Technology Hyderabad, Andhra Pradesh – 502205, India
[2]*Department of Materials Science and Metallurgical Engineering,*
Indian Institute of Technology Hyderabad, Andhra Pradesh – 502205, India
[*]Author for Correspondence: asthanas@iith.ac.in

ABSTRACT

The polycrystalline $Bi_{1-x}Eu_xFeO_3$ (x = 0, 0.05 and 0.1) ceramics were synthesized by conventional solid-state route. X-ray diffraction studies and Raman measurements revealed that the compounds crystallized in rhombohedral structure with *R3c* space group. In addition, a nominal percentage of orthorhombic phase was observed in 10 mole% Eu substituted $BiFeO_3$. Appearance of weak ferromagnetism and significant increase in Néel temperature T_N in the substituted

compounds were discussed on the basis of structural distortions. Enhanced remnant magnetization of 75 memu/g and large coercive field of 6.4 kÖe were observed in 10 mole% Eu substituted $BiFeO_3$. Equivalent circuit model was employed to estimate the grain and grain boundary contributions towards the electrical parameters such as resistance, conductivity etc. Non-Debye type of relaxation was confirmed from impedance and electric modulus studies. The obtained frequency variation of ac conductivity at different temperature obeys Jonscher's power law and is consistent with the correlated barrier hopping (CBH) model. Temperature variations of ac conductivity explained that electronic hopping, oxygen vacancies movement and/or creation of defects contribute to conduction in all the compounds.

I. INTRODUCTION

Materials which have simultaneous existence of ferroic orders such as ferroelectric, (anti)ferromagnetic and or ferroelastic are called multiferroics. These materials are potential candidates for device applications such as memory devices, microelectronics and spintronics.[1,2] Among all materials, $BiFeO_3$ (BFO) is fascinating and well-studied for several decades. BFO has high Curie temperature (T_C = 1103 K) and high Néel temperature (T_N = 643 K).[3,4] In bulk form, its crystal structure stabilizes in rhombohedral structure with *R3c* space group. Ferroelectricity arises due to the distortion induced by stereochemically active $6s^2$ lone pair electrons of Bi^{3+}, while the indirect magnetic exchange interaction between Fe^{3+} ions through O^{2-} causes G-type antiferromagnetic ordering. This G-type antiferromagnetic ordering is superimposed with space modulated spiral structure (SMSS) of incommensurate wavelength 62 nm. However, synthesis of single phase BFO is a challenging task. Presence of oxygen vacancies, mixed valence states of Fe ions, impurity phases such as $Bi_2Fe_4O_9$, $Bi_{25}FeO_{40}$ enhance the electrical conductivity which is a serious drawback for device applications.[5] To minimize the impurity phases and to reduce the leakage currents, various attempts have been made such as i) adopting several processing techniques,[6-8] (ii) substitution of elements at Bi/Fe – site,[8, 9] (iii) fabricating composites.[10] The most effective technique to tune the multiferroic properties is to create internal chemical pressure with the substitution of elements at A-site or B-site. Lanthanides[7,8] and IIA alkaline earth metals[6] are substituted at A-site where as transition metals elements are substituted at B- site.[11] Substitution of divalent ions at A- site increases the oxygen vacancies[6] in order to maintain charge neutrality. This enhances the leakage current which leads to deterioration of electrical properties of the compounds. Partial substitution of lanthanides at Bi - site not only effectively minimizes the impurity phases and reduces the leakage current, but also improves both magnetic and electric properties of BFO. While extensive studies on structural, magnetic, dielectric and ferroelectric

properties of lanthanide substituted BFO have been done, there have been very few reports on conductivity studies and electric transport mechanism on this compound.[8, 12-15]

Macroscopic electrical properties of polycrystalline ceramics are determined by microstructure such as grain and grain boundary distributions in the compound. To investigate the electrical properties of polycrystalline ceramics, impedance spectroscopy is the most versatile tool. These studies, over a wide range of frequency and temperature, will assist to assess the insulating character of the compound for potential application.

In this communication, Eu is used as a substitute for Bi in BFO and its structural, magnetic and electrical transport properties of resultant compound are studied. Eu is used as a substitute because; i) smaller ionic size of Eu creates internal chemical pressure which distorts FeO_6 octahedra and changes Fe – O – Fe bond angle and Fe – O bond distances. These changes suppress the SMSS which induces weak ferromagnetism [8,9] and ii) the bond enthalpy of Eu - O bond (475±10 kJ/mol) is greater than that of Bi - O bond (337±12.6 kJ/mol).[16-18] Stronger bond enthalpy of R - O bond (R = Rare earth) compared to Bi – O bond presumably reduces oxygen vacancies[19,20] and improves insulating character which is essential in terms of the potential applications. Further, it is also observed from our UV-Vis-NIR spectrophotometry studies (not shown here) that band gap increases with Eu substitution which also supports the improved insulating character in the substituted compounds.

II. EXPERIMENTAL

$BiFeO_3$ (BFO) and $Bi_{1-x}Eu_xFeO_3$ (BEFO) [x = 0.05 (BEFO5), 0.1 (BEFO10)] polycrystalline compounds were synthesized by conventional solid-state reaction using the high purity Bi_2O_3 (99.999%, Sigma-Aldrich, USA), Fe_2O_3 (99.98%, Sigma-Aldrich, USA) and Eu_2O_3 (99.9%, Sigma-Aldrich, China) as starting materials. These powders were weighed in stoichiometric proportions and ground thoroughly for 2 hrs. Ground powders were calcined at 780 °C for 2 hrs and then at 815 °C for 3 hrs. After calcination, the powders were mixed with PVA and pressed uniaxially in to pellets with 8 mm diameter and 1.5 mm thickness. These pellets were finally sintered at 830°C for 3 hrs. Phase analysis of the compounds was confirmed by using X-ray diffractometer (Panalytical X'pert Pro) with Cu K_α radiation (λ = 1.5406 Å) with the step size of 0.0167° over the angular range $20° \leq 2\theta \leq 90°$. Microstructure characterization and compositional analysis (EDAX) were carried out using field emission scanning electron microscopy (FESEM, Carl Zeiss, Supra 40). Raman scattering studies were performed on polished pellet using a laser micro Raman spectrometer (Bruker, Senterra) with an excitation source of 785 nm. The magnetic properties were measured using PPMS with VSM assembly (Quantum Design, USA). Differential

scanning calorimetry (DSC) was performed using a TA-Q200 calorimeter at a heating rate of 10 °C/min under N_2 atmosphere. Dielectric property assessments were performed on the compounds with silver electrode using Wayne Kerr 6500B impedance analyzer.

III. RESULTS AND DISCUSSIONS

Fig. 1(a) shows the XRD patterns of BFO and BEFO compounds. Trace amounts of impurity phases such as $Bi_{25}FeO_{40}$ and $Bi_2Fe_4O_9$ were observed along with the main phase.[4] Rietveld refinement[21] revealed that, all compounds were crystallized in the rhombohedral crystal structure with *R3c* space group. However, an evolution of nominal percentage of orthorhombic phase with *Pnma* space group was evident in BEFO10 compound. As shown in Fig. 1(b), with the increase of Eu substitution, two Bragg's peaks (104) and (110) shifted towards higher angle side and partially overlapped. The relative intensity of (104) peak gradually decreased compared to (110) peak intensity. Meanwhile, the intensity of a peak (006) at 37.6° which originates from rhombohedral structure became weaker with Eu content. Moreover, a weak (111) reflection near 25.4° (marked by an arrow) in BEFO10 compound is commonly observed which corresponds to *Pnma* phase.[6]

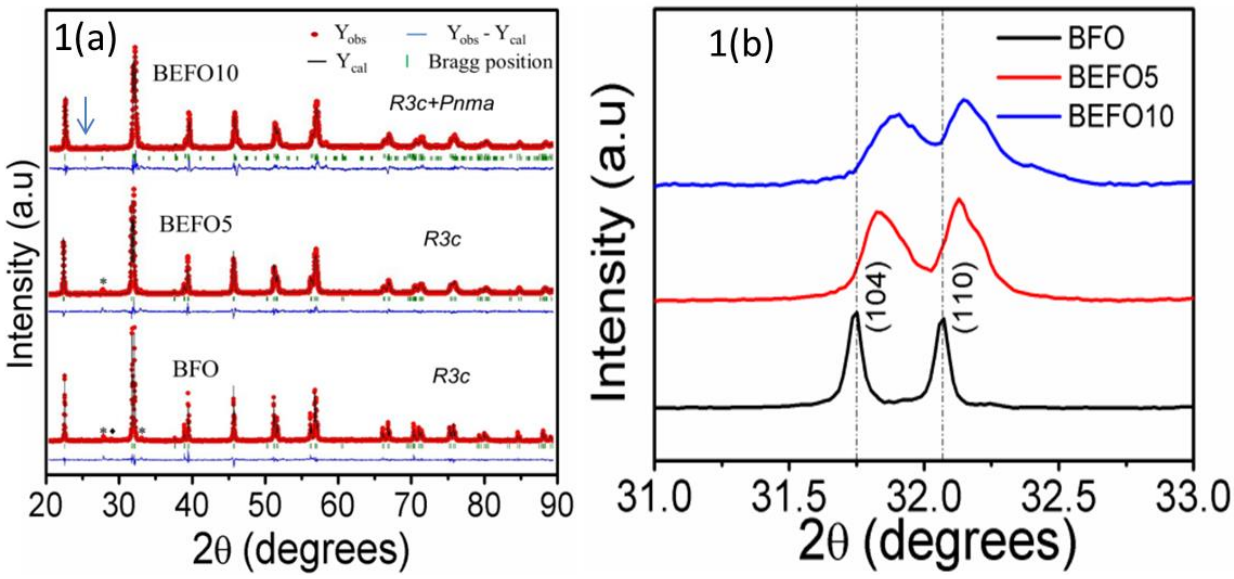

FIG. 1. (a) XRD patterns of BFO and BEFO compounds. ♦ and ∗ represent impurity phases corresponding to $Bi_{25}FeO_{40}$ and $Bi_2Fe_4O_9$ respectively. Arrow shows weak (111) reflection near 25.4° in BEFO10 compound (b) XRD patterns of BFO and BEFO compounds near 31-33 °.

This clearly indicates that Eu substitution results in evolution of orthorhombic phase within the major rhomobohedral phase. Coexistence of such *Pnma* phase with *R3c* phase was also reported in the literature[22] and also supported from our Rietveld refinement. Evolution of orthorhombic

phase could be explained on the basis of internal chemical pressure using Goldschmidt tolerance factor *t*, defined as $t = (\langle r_A \rangle + r_O)/\sqrt{2}(r_B + r_O)$ where <r_A> is the average radius at A-site and r_B and r_O are the radii of Fe^{3+} and O^{2-} respectively. The tolerance factor decreased with the Eu content. The decrement in *t* leads to Fe^{3+} - O and Bi^{3+} / R^{3+} - O bonds under compression and tension respectively. Cooperative rotation of oxygen octahedra takes place in order to reduce the induced lattice stress.[23] Substitution of relatively smaller size of Eu ion increases the relative rotation angle of oxygen octahedra along the polarization direction which is [111] axis. This induced lattice distortion suppresses the rhombohedral phase with the evolution of preferable lower symmetric phases. The internal chemical pressure induced structural distortion modifies the Fe-O-Fe bond angles and the Fe-O bond distances which are responsible for tuning multiferroic properties of BFO. The lattice parameters, volume of the unit cell, bond angle and bond distance of BFO and BEFO compounds with the reference of R3c phase (major-phase) are given in Table I.

Table I. Variation of the lattice parameters, volume of the unit cell, bond angle and bond distance of BFO and BEFO compounds.

Composition	a_{hex} (Å)	c_{hex} (Å)	V (Å)^3	Fe-O-Fe	Fe-O1(Å)	Fe-O2(Å)
$x = 0$	5.5794 (6)	13.8709 (6)	373.95(6)	153.2(7)	2.215(16)	1.860(17)
$x = 0.05$	5.5734 (6)	13.8393 (6)	372.30(3)	154.4(6)	2.125(15)	1.935(13)
$x = 0.10$	5.5714 (5)	13.8239 (8)	371.62(1)	156.9(9)	2.061(18)	1.980(2)

Scanning electron micrographs of BFO and BEFO compounds are shown in Fig. 2. It can be seen that BFO has an average grain size around 9 μm with a few distinct pores. The effect of Eu substitution on the grain size was clearly evident from the micrographs.

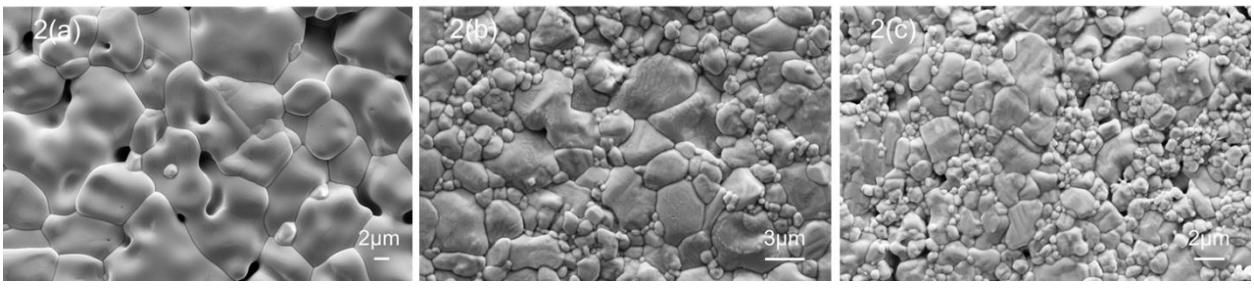

FIG. 2. FESEM micrographs of (a) BFO, (b) BEFO5 and (c) BEFO10 compounds.

Table II. Density, average grain size and grain size distribution and activation energies of BFO, BEFO5 and BEFO10 compounds.

Compound	% of relative density	Average grain size (μm)	Grain size distribution (μm)	Activation energy *E* (eV) from		
				σ_{dc} data for	M'' vs ω data	$ln\sigma_{ac}$ vs *1000/T* data at 100 kHz

				Grain	Grain boundary		Region I	Region II	Region III
BFO	88	9	1.5-9.5	0.76	1.00	0.69	0.18	0.59	1.38
BEFO5	91	2	0.5-4.0	0.74	0.88	0.74	0.21	0.54	1.42
BEFO10	93	1	0.5-3.5	0.88	0.95	0.75	0.16	0.67	1.63

Eu substitution decreased the grain size, reduced porosity and improved the density of the compounds. Densities of the compounds were measured by Archimedes principle. Density, average grain size and grain size distribution of BFO, BEFO5 and BEFO10 compounds are given in Table II. Improved density in BEFO compounds leads to better grain connectivity with reduced porosity which was confirmed from the microstructural analysis. Eu^{3+} ions suppress the grain growth due to their lower diffusivity which in turn decreases the grain size[24] From energy dispersive x-ray spectrum (not shown here), all the compounds showed Bi:Fe ratio approximately 1:1.

Raman spectra of BFO and BEFO compounds are shown in Fig. 3(a). The natural frequency of each Raman active mode was obtained by fitting the spectra and de-convoluted them into individual modes. According to the group theory, BFO with rhombohedral *R3c* symmetry has 13 Raman modes which can be represented in irreducible notation as $\Gamma = 4A_1+9E$.[25,26] The letter *A* represents the symmetric transformation of a molecule under the rotation about the principle axis of symmetry. The letter *E* represents a twofold degenerate vibration. The low frequency modes at 139, 172 and 231 cm^{-1} were assigned as A_1-1, A_1-2 and A_1-3 respectively. The remaining peaks at 129, 261, 276, 303, 346, 369, 432, 480 and 524 cm^{-1} were assigned as *E* modes[27,28] and all these modes are given in Table III. It is reported that in BFO, A_1 modes at 139, 172 and 231 cm^{-1} and *E* modes with frequencies less than 400 cm^{-1} are attributed to Bi – O bonds whereas the E modes with frequencies greater than 400 cm^{-1} are attributed to Fe – O bonds.[29] Fig. 3(b) shows A_1 and *E* modes of BFO and BEFO compounds between 100 and 200 cm^{-1}. In real crystals, life times of phonons are reduced due to the scatterings from defects, disorder, strain etc. The decrease in life times of phonons leads to increase in FWHM as FWHM is inversely proportional to life times. Substitution of Eu at Bi – site leads to A- site disorder which in turn increases the peak broadening (FWHM) and decreases the intensity of the peak.[30,31] The two strongest A_1 modes at 139 and 172 cm^{-1} show blue shift due to the substitution of less atomic mass element (Eu) at Bi site.[32]

From these findings, it can be concluded that the Eu^{3+} ion replaces Bi^{3+} ion at A-site of host BFO lattice. The *E* modes of BFO at 261, 276, 346, 369 cm^{-1} respectively shifted to 262, 280,

338 and 375 cm^{-1} with the increase of Eu substitution which corresponds to evolution of orthorhombic phase.[22] Further, the gradual hardening of *E* modes at 276 and 303cm^{-1} due to variation in internal chemical pressure may be attributed to the destabilization of Fe cations and the octahedral tilts as reported by Yang et al[33] in pressure induced studies. The changes in *E* modes with Eu-content as discussed above indicate the evolution of orthorhombic phase which is also supported from XRD analysis.

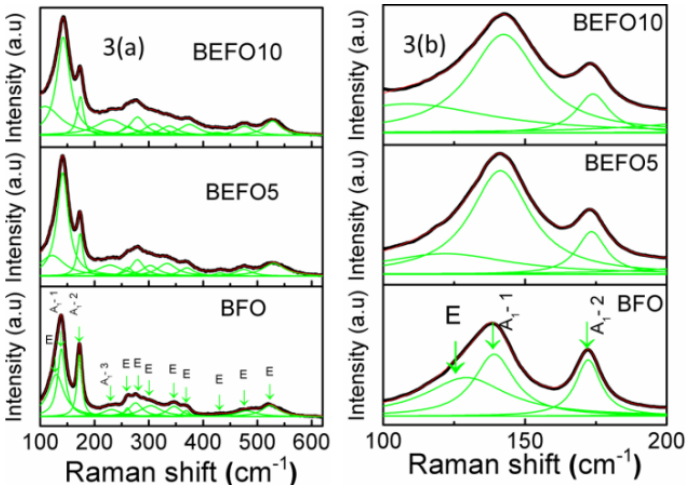

FIG. 3. (a) Raman spectra of BFO and BEFO compounds and (b) A_1 and E modes of BFO and BEFO compounds between 100 and 200 cm^{-1}.

Table III. Raman modes (cm^{-1}) of BFO and BEFO compounds.

Raman mode (cm^{-1})	**BFO**	**BEFO5**	**BEFO10**
E	129	122	109
A_1-1	139	141	142
A_1-2	172	173	174
A_1-3	231	228	229
E	261	261	262
E	276	279	280
E	303	303	309
E	346	339	338
E	369	370	375
E	432	431	426
A_1-4	480	475	476
E	524	530	528

Fig. 4(a) shows the magnetization hysteresis loops of BFO and BEFO compounds at 300K. BFO exhibits G-type antiferromagnetic structure (i.e., each Fe^{3+} ion is surrounded by six nearest neighbours with antiparallel spins). G-type antiferromagnetic structure is superimposed with a spiral spin structure of incommensurate wave length of 62 nm[34] which cancels the net

magnetization and inhibits the linear magnetoelectric effect in bulk BFO.[35] Variation of remnant magnetization M_r and coercive field H_c with Eu substitution are given in Table IV.

Non-saturation in magnetization was observed up to the applied field of 5 kÖe which indicates that all the compounds retained the intrinsic antiferromagnetic nature. However, with the increase in Eu content, the spin structure (SMSS) was suppressed due to variations in Fe-O bond distances and bond angles,[36] which leads to appearance of weak ferromagnetism.

TABLE IV. Remnant magnetization M_r and coercive field H_c of BFO and BEFO compounds.

Compound	M_r (memu/g)	H_c (kÖe)
BFO	0.626	0.235
BEFO5	21	2.4
BEFO10	75	6.4

Enhanced magnetization and coercive field in BEFO10 compound are not due to the presence of $Bi_2Fe_4O_9$ and $Bi_{25}FeO_{40}$ impurities phases which are paramagnetic at room temperature. Further, it is worth to mention that remnant magnetization (M_r = 0.075 emu/g) increased by two orders of magnitude in BEFO10 compared to BFO. This large change in M_r could be due to the presence of minor orthorhombic phase which in turn leads to the more pronounced suppression of SMSS in BEFO10[23]. Based on the above discussion, the appearance of weak ferromagnetism in the studied compounds can be attributed to the suppression of SMSS.

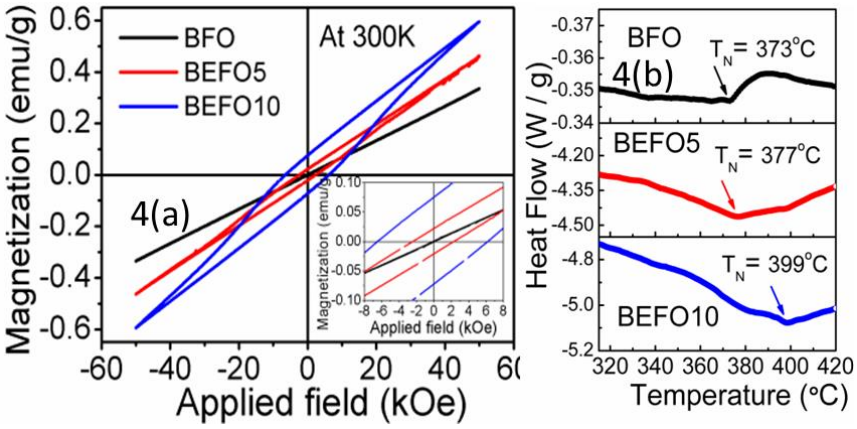

FIG. 4. (a) Isothermal magnetization plots of BFO and BEFO compounds at 300K. Inset shows the enlarge view (b) Differential scanning calorimeter plots of BFO and BEFO compounds.

Differential scanning calorimeter (DSC) plots of BFO and BEFO compounds are shown in Fig. 4(b). All DSC curves showed a minimum which correspond to a second order antiferromagnetic – paramagnetic transition. For BFO, Néel temperature (T_N) is observed to be

373ºC which is well matched with the reported values.[5] An increase in Néel temperatures was observed for BEFO5 (T_N = 377ºC) and BEFO10 (T_N = 399ºC) compounds. However, K. Deepti et al[37] noticed insignificant changes in T_N whereas W. H. Sung et al[38] reported decrease in T_N in Eu-substituted BFO. The variation of T_N with Fe – O – Fe bond angle can be explained by the following equation.[8,39]

$$T_N = JZS(S+1)\cos\theta \quad (1)$$

Where J is the exchange constant, S is the spin of Fe^{3+}; Z is the average number of linkages per Fe^{+3} ions and θ is Fe – O – Fe bond angle. As the Eu content increased, the bond angle also increased from153.2º (x = 0) to 156.9º (x = 0.1). In the above equation, T_N is proportional to the cosine of bond angle which increases with bond angle. Further, due to stronger bond enthalpy of Eu – O compared to Bi – O bond, number of oxygen vacancies might be suppressed which may lead to increase in Z towards ideal value of 6. Based on the above discussion, increase in T_N is expected and is in consistent with our observations. This can also be expected due to high Néel temperature of $EuFeO_3$ compound.[40]

Frequency variation of real part of impedance (Z′) of BFO and BEFO at different temperatures are shown in Fig. 5(a) – (c). Presence of dielectric relaxation behaviour was evident from the dispersion behaviour of Z' in the low frequency regions. Decrement in Z' with frequency was due to the increase of hopping of charge carrier which leads increased ac conductivity. Negative temperature coefficient of resistance (NTCR) character could be accounted in terms of decrement in Z' with temperature. Increase in Z' with Eu substitution indicated that the bulk resistance was improved.[8,41] This may be due to increase in the effective potential barrier heights with the structural distortions.[15] Further, from our UV-Vis-NIR spectrophotometry studies, increase in band gap of BFO (2.05 eV) with Eu substitution (not given here) towards the band gap of $EuFeO_3$ (3.69 eV)[41] supports the above conclusion.

The temperature variation of complex impedance can be understood using the following equations[43,44]

$$Z^* = Z_o(T)\int \frac{y(\tau,T)d(\tau)}{1+j\omega\tau} \quad (2)$$

Real and imaginary parts of complex impedance can be expressed as

Real part: $$Z'(\omega,T) = Z_o(T)\int \frac{y(\tau,T)d(\tau)}{1+\omega^2\tau^2} \quad (3)$$

and imaginary part: $$Z''(\omega,T) = Z_o(T)\int \frac{(\omega\tau)^* y(\tau,T)d(\tau)}{1+\omega^2\tau^2} \quad (4)$$

Where ω is the angular frequency, τ is the relaxation time and $y(\omega, \tau)$ represents distribution of relaxation times.

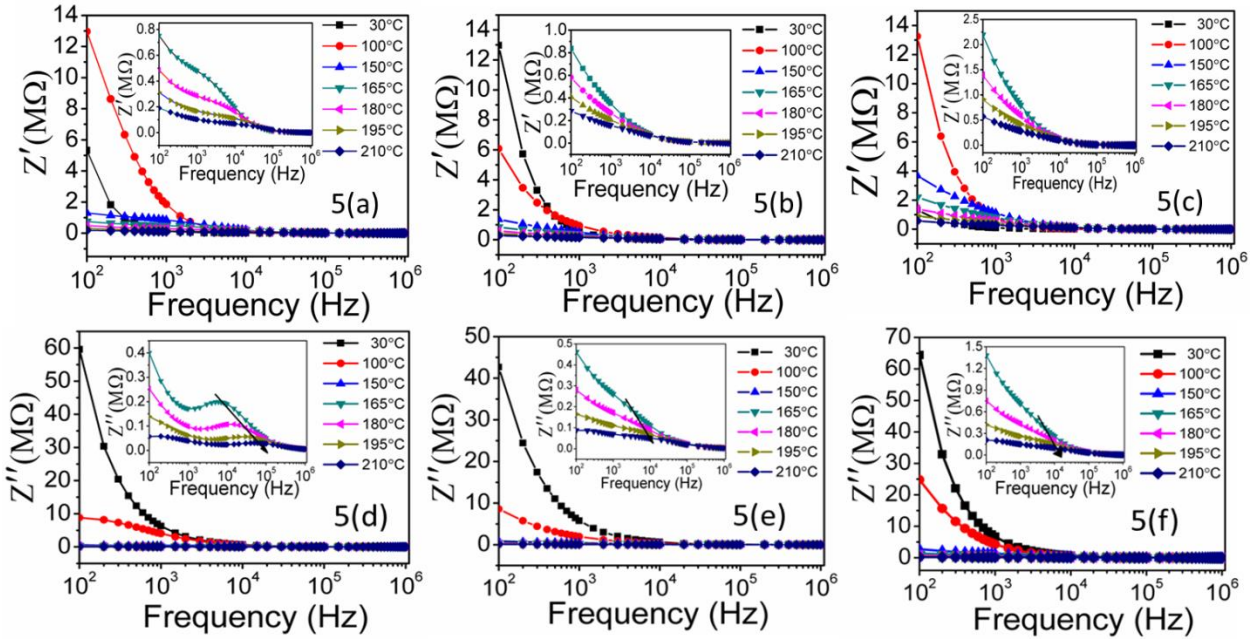

FIG. 5. Frequency variation of real part of impedance (Z′) for (a) BFO, (b) BEFO5 and (c) BEFO10 compounds. Frequency variation of imaginary part of impedance (Z″) for (d) BFO, (e) BEFO5 and (f) BEFO10 compounds. Insets in figures 5 (a) – (c) and 5 (d) – (f) show the frequency variation of Z′ and Z″ from temperature 165 °C to 210 °C respectively.

Fig. 5(d) – (f) shows frequency dependence of the imaginary part of impedance (Z″) of BFO and BEFO compounds. Above 165 °C, Z″ data is characterized by i) appearance of a peak with a maximum value (Z''_{max}) at a certain frequency, ii) asymmetrical broadening, iii) shifting of Z''_{max} value to higher frequency with the increase in temperature and iv) decrement of magnitude of Z''_{max} with the temperature. Appearance of peak indicates the presence of electrical relaxation in the compounds. Asymmetric broadening suggests that there is a distribution of relaxation times. Shifting of Z''_{max} value to higher frequency with temperature indicates that these relaxations are temperature dependent.[8] In Eu substituted BFO compounds, Z″ peak became weak which is due to the presence of indistinguishable relaxation times corresponding to grain and grain boundaries.

Generally, polycrystalline dielectric materials have grains separated by interfacial boundary layers (grain boundaries). The corresponding features can be seen with two semi-circular arcs in the complex impedance plots. Each semi-circular arc can be modelled in terms of electrical equivalent circuit consisting of a parallel combination of a resistor *R* and a capacitor (or constant phase element CPE) *C* as shown in Fig. 6. The impedance of the resultant circuit[45] can be expressed as

$$Z^* = \frac{R_g}{1+(j\omega R_g C_g)^{n_g}} + \frac{R_{gb}}{1+(j\omega R_{gb} C_{gb})^{n_{gb}}} \quad (5)$$

Where R_g and R_{gb} are grain and grain boundary resistance, C_g and C_{gb} are grain and grain boundary capacitances and n_g and n_{gb} are relaxation time distribution functions respectively. The value of n is a measure of deviation from ideal Debye behaviour. For an ideal Debye relaxation, n should be unity[46] and in reality its value varies from zero to unity.

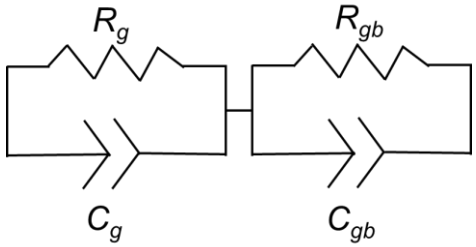

FIG. 6. Schematic picture of parallel combination of resistor and capacitor for grain and grain bondary.

The observed data was fitted with two equivalent *R*-*C* parallel circuits corresponding to grain and grain boundary effects as shown in Fig. 7. Presence of a single semi-circle arc indicates that electrical relaxations in the material arise basically from the bulk material. Appearance of second semi-circular arc in the low frequency region is due to the grain boundary effects. The low frequency semi-circular arc is corresponding to the grain boundary and high frequency semi-circular arc is corresponding to the grain. Each semi-circular arc can be ascribed as a parallel combination of resistance, *R* and capacitance (or constant phase element CPE) *C*. The assignment of these two semi-circular arcs to the electrical response due to grain interior and grain boundary is consistent with the ‘‘brick-layer model’’.[47]

If there exits multi-relaxations in the material, the semi-circular arcs are depressed i.e. dielectric relaxation deviates from ideal Debye relaxation behaviour. As the temperature increases, the circular arc depresses, and the intercept of arc with the Z' axis shifts towards the origin in the Nyquist plots. Shifting of intercept towards origin indicates decrease in bulk resistance of the compound. The values of R_{gb} (grain boundary resistance) and R_g (grain resistance) were estimated by fitting the Nyquist plots from 150 ^{o}C to 225 ^{o}C for all the compounds. With the increase in temperature from 150 ^{o}C to 225 ^{o}C, the values of R_{gb} and R_g decreased respectively from 8.4 MΩ to 1 MΩ and 0.9 MΩ to 42 kΩ for BFO, 5 MΩ to 0.18 MΩ and 1 MΩ to 66 kΩ for BHFO5 and 10 MΩ to 0.31 MΩ and 3 MΩ to 83 kΩ for BHFO10 compounds. This indicates that the compounds showed NTCR character which is consistent with the Z' data. Grain boundary resistance dominated over grain resistance at all temperatures for all the compounds. The value of grain resistance increased with the substitution of Eu at any temperature. This indicates the improvement in the barrier properties for the flow of charge carriers with the Eu substitution.

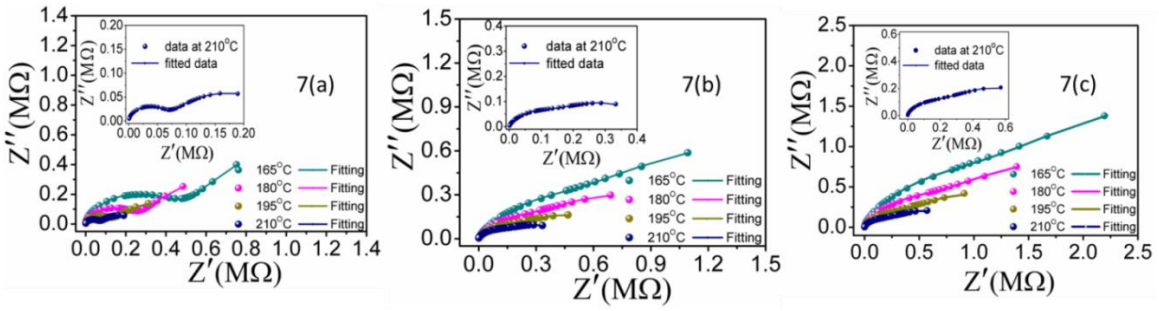

FIG. 7. Nyquist plots of (a) BFO, (b) BEFO5 and (c) BEFO10 compounds at different temperatures.

DC conductivity of the compounds were calculated from the equation,

$$\sigma_{dc} = \frac{t}{AR} \tag{6}$$

Where t is the thickness of the pellet, R is the resistance (of the grain or grain boundary) of the compound and A is the area of the electrode. Both grain and grain boundary conductivities increased with the increase in temperature and followed Arrhenius relation. The activation energies were obtained from the linear fitting of plot drawn between $ln\sigma_{dc}$ and $1000/T$. The activation energies of grain and grain boundaries of BFO and BEFO compounds were given in Table II.

Complex electric modulus $M^*(\omega)$ formalism is a powerful technique to study the electrical response of the material. The electric modulus (M^*) is expressed as

$$M^* = M' + iM'' = i\omega C_o Z^*$$
$$= i\omega C_o (Z' - iZ'') = \omega C_o Z'' + i\omega C_o Z' \tag{7}$$

Where ω is the frequency of applied electric field and C_o is the capacitance in vacuum. Frequency variation of real part of electric modulus (M') plots of BFO, BEFO5 and BEFO10 compounds at different temperatures are shown in Fig. 8(a) – (c). M' plot is characterized by very small value (close to zero) at the low frequency region and increases with the increase in frequency at all temperatures, indicating negligible electrode polarization phenomenon in the test material.[48] M' showed the dispersion which increased with the increase in frequency and shifted towards the higher frequency side. Frequency variation of imaginary part of electric modulus (M'') at different temperatures for BFO and BEFO compounds are shown in Fig. 8(d) – (f). The value of electric modulus (M'') was calculated using the formula

$$M'' = \omega C_O Z' \tag{8}$$

Frequency variation of M'' curves are characterized by i) appearance of peak at unique frequency, at a given temperature, ii) significant broadening in the peak which indicates the presence of distribution of relaxation times and hence the relaxation is of non-Debye type and iii) shifting of

peak position towards high frequency region with the rise of temperature which indicates the relaxation process is thermally activated.

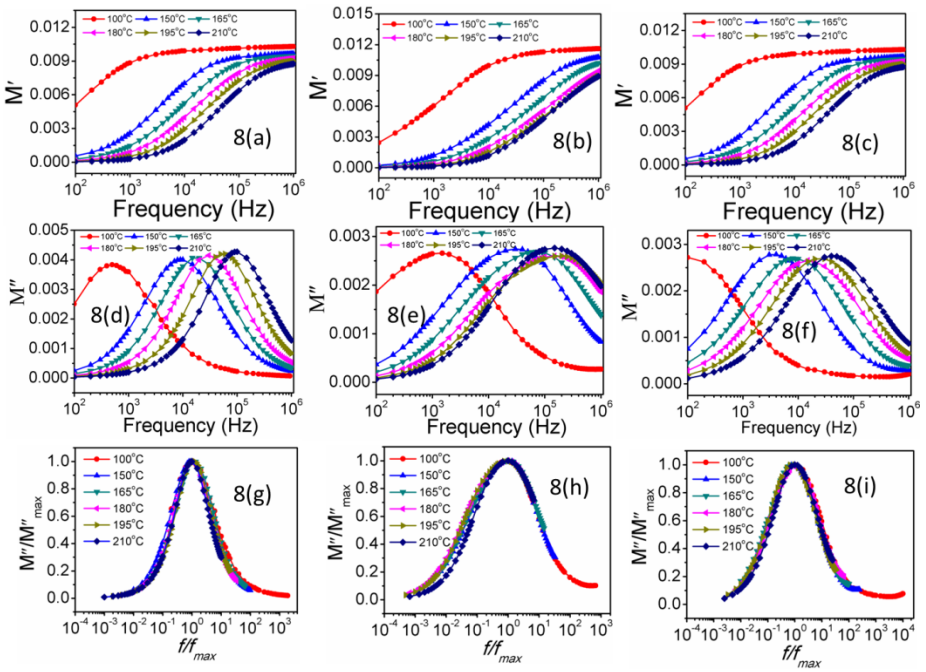

FIG. 8. Frequency variation of real part of complex electric modulus (M') plots for (a) BFO,(b) BEFO5 and (c) BEFO10 compounds. Frequency variation of imaginary part of complex electric modulus (M'') plots for (d) BFO,(e) BEFO5 and (f) BEFO10 compounds. Modulus master curves (M''/M''_{max} vs f/f_{max}) for (g) BFO, (h) BEFO5 and (i) BEFO10 compounds.

The frequency region below the maximum value of M'' (M''_{max}) indicates the range of frequencies for the charge carriers to perform long range hopping from one site to another site where as frequencies above M''_{max}, charge carriers perform short range hopping and these particles are confined to their potential wells. The frequency ($\omega_{\max}$) corresponding to the M''_{max} gives the most probable relaxation time (τ_{max}) for the charge carriers and follows the Arrhenius law

$$\omega_{\max} = \omega_o e^{-E_a/kT} \tag{9}$$

Where ω_o is the pre exponential factor and E_a is the activation energy. The activation energies of BFO and BEFO compounds, calculated from the slope of the plot drawn between $ln(\omega_{max})$ and $1000/T$, are given in Table II.

Variation of normalized imaginary part of electric modulus (M''/M''_{max}) with normalized frequency (f/f_{max}) for BFO and BEFO compounds are shown in Fig. 8(g) – (i). For a given compound, all curves at different temperature merge on a single master curve which indicates that all the dynamic processes occurring at these temperatures will have the same activation energy.

Fig. 9 shows the frequency dependence of ac conductivity of BFO and BEFO compounds at different temperatures. The response of the material to the applied electric field is described by

the ac conductivity. These studies will be useful to investigate the nature of transport process in the compounds.

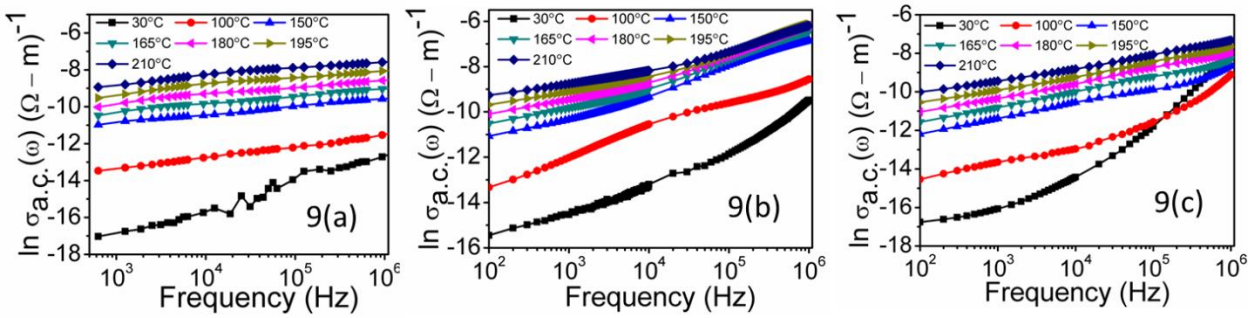

FIG. 9. Frequency variation of ac conductivity of (a) BFO, (b) BEFO5 and (c) BEFO10 compounds.

The ac electrical conductivity was calculated by using the relation,

$$\sigma_{a.c} = \varepsilon_o \varepsilon_r \omega \tan\delta \tag{10}$$

The frequency dependence of ac conductivity obeys Jonscher's power law[49]:

$$\sigma_{a.c} = \sigma(0) + A\omega^s$$
$$= \sigma(0) + \sigma(\omega) \tag{11}$$

Where σ (0) is the dc conductivity and s is an exponent.

The frequency dependence part $\sigma(\omega)$ is generally explained on the basis of two mechanisms. In the case of quantum mechanical tunnelling (QMT) through the barrier separating the two localized sites, the value of s should be independent of temperature and should slightly decrease with frequency[50] while in the case of correlated barrier hopping (CBH), s should decrease with increase in temperature.[51] It was observed that, for BFO and BEFO compounds, s values decreased with increase in temperature. Therefore, the observed data was consistent with the CBH model and the conduction process was thermally activated.

Fig. 10 shows the Arrhenius plots of ac conductivity at different frequencies for BFO and BEFO compounds. The temperature dependence of ac conductivity can be represented by the Arrhenius equation

$$\sigma_{a.c} = \sigma_o \exp(-E/kT) \tag{12}$$

Where σ_o is the electric conductivity at infinite temperature, k is the Boltzmann constant and E is the activation energy. The activation energies were calculated at frequencies 1 kHz, 10 kHz, 100 kHz, 500 kHz and 1 MHz for BFO and BEFO compounds. The obtained values at 100 kHz for all compounds were given in Table II.

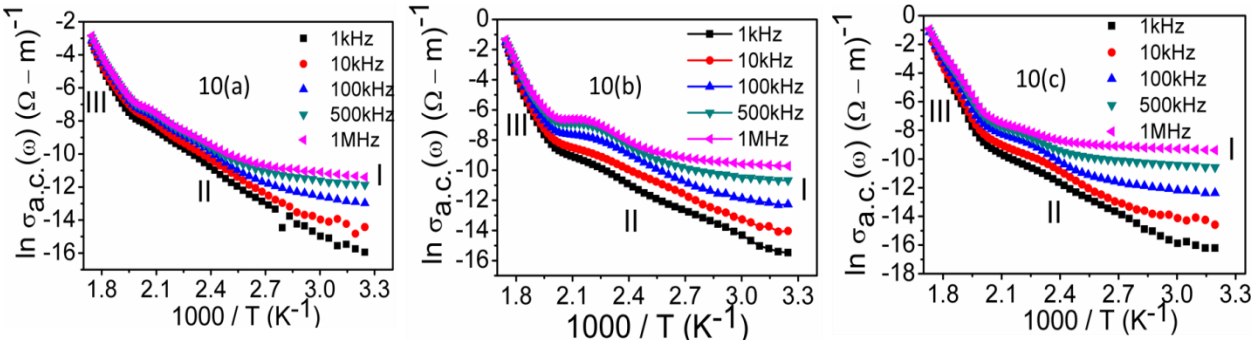

FIG. 10. Temperature dependence of ac conductivity of (a) BFO, (b) BEFO5 and (c) BEFO10 compounds.

In region I (below 393K), conductivity was frequency dependent, but temperature independent. The ac conductivity increased with the increase of frequency due to the increase of hopping of charge carriers. In this region, strong frequency dispersion was observed in all the three compounds. Activation energies were found to be decrease with increase in frequency. Low activation energies were observed and attributed to the electronic hopping conduction. In region II (393K – 503K), conductivity not only depends on temperature, but also on frequency. Contribution of short range of oxygen vacancies to the conductivity is expected in this region. In region III (503K – 573K), conductivity was frequency independent and temperature dependent. Conductivity was attributed to long range movement of oxygen vacancies or creation of defects.[14] Increase in activation energies were found with the increase in temperature.

IV. CONCLUSIONS

The polycrystalline $Bi_{1-x}Eu_xFeO_3$ (x = 0, 0.05 and 0.1) compounds were synthesized by conventional solid-state route. Compounds were crystallized in rhombohedral structure with *R3c* space group. Further, a nominal percentage of orthorhombic phase with *Pnma* space group was observed in 10mole% Eu substituted $BiFeO_3$. Magnetization measurements showed that weak ferromagnetism and significant increase in Néel temperature in Eu substituted compounds were mainly due to the crystal distortions. Insulating character of $BiFeO_3$ compound improved with Eu substitution which is evident from the impedance studies. The obtained ac conductivity data obeys Jonscher's power law and is consistent with the correlated barrier hopping (CBH) model. The observed activation energies conclude that electronic hopping, oxygen vacancies movement and creation of defects are the contributors to the ac conductivity.

ACKNOWLEDGEMENTS

Authors are grateful to the Department of Science and Technology (DST), Government of India for their financial support under Fast Track scheme (SR/FTP/PS–065/2011) to carry out this work.

[1]W. Eerenstein, N. D. Mathur, and J. F. Scott, Nature **442,** 759 (2006).

[2] G. Catalan, and J. F. Scott, Adv. Mater. **21,** 2463 (2009).

[3]K. F. Wang, J. M. Liu, and Z. F. Ren, Adv. Phys. **58,** 321 (2009).

[4]Wang Jet al, Science, **299,** 1719 (2003).

[5]V. R. Palkar, J. John, and R. Pinto, Appl. Phys. Lett. **80,** 1628 (2002).

[6]X. K. Chen, Y. J. Wu, J. Zhang, and X. J. Chen, Sci China-Phys Mech Astron. **55,** 404 (2012).

[7] T. D. Rao, T. Karthik, and S. Asthana, J Rare Earths, **31,** No. 4 370 (2013).

[8]T. D. Rao, T. Karthik, A. Srinivas, and S. Asthana, Solid State Comm., **152,** 2071(2012).

[9]F. Chang, N. Zhang, F. Yang, S. Wang, and G. Song, J. Phys. D: Appl. Phys. **40,** 7799 (2007).

[10]D. H. Wang, W. C. Goh, M. Ning, and C. K. Ong, Appl. Phys. Lett. **88,** 212907 (2006).

[11]B. C. Luo, C. L. Chen, and K. X. Jin, Solid State Comm., **151,** 712 (2011).

[12]R. Schmidt, W. Eerenstein, T. Winiecki, F. D. Morrison, and P. A. Midgley, Phys. Rev. B **75**, 245111 (2007).

[13]K Sardar, J. Hong, G. Catalan, P. K. Biswas, M. R. Lees, R. I. Walton, J. F. Scott, and A. T. S. Redfern J. Phys.: Condens. Matter **24,** 045905 (2012).

[14]P. Pandit, S. Satapathy, and P. K. Gupta, Physica B, **406,** 2669 (2011).

[15]A. Mukherjee, S. Basu, G. Chakraborty, and M. Pal, J. Appl. Phys., **112,** 014321 (2012).

[16]J.A. Kerr in 1999-2000: CRC Handbook of Chemistry and Physics, 81st edn (CRC Press, Boca Raton, Florida, USA, 2000).

[17]J. B. Pedley, E. M. Marshall, J. Phys. Chem. Ref. Data **12** (1983).

[18]M. Dulick, E. Murad, R. F. Barrow, The Journal of Chemical Physics **85**, 385 (1986).

[19]Woo-Hee Kim, Jong Yeog Son, Appl. Phys. Lett. **103,** 132907 (2013)

[20]I Coondoo, N Panwar, I Bdikin, V S Puli, R. S. Katiyar, A. L. Kholkin, J. Phys. D: Appl. Phys. **45,** 055302 (2012).

[21]J. Rodrigues-Carvajal, FULLPROF. A Rietveld Refinement and Pattern Matching Analysis Program (Laboratoire Leon Brillouin, CEA-CNRS, France, 2000).

[22]Y. A. Zheng, Y. J. Wu, Z. X. Qin, and X. J. Chen, Chin. J. Chem. Phys, **26,** 2 (2013).

[23]X. Q. Zhang, Y. Sui, X. J. Wang, Y. Wang, and Z. Wang, J. Alloys Compd., **507,** 157 (2010).

[24]X. Chou, J. Zhai, H. Jiang, and X. Yao, J. Appl. Phys. **102,** 084106 (2007).

[25]R. Haumont, J. Kreisel, P. Bouvier, and F. Hippert, Phys. Rev. B, **73,** 132101 (2006).

[26]H. Fukumura, H. Harima, K. Kisoda, M. Tamada, Y. Noguchi, and M. Miyayama, J. Magn. Magn. Mater. **310,** 367 (2007).

[27]Y. Yang, J. Y. Sun, K. Zhu, Y. L. Liu, and L. Wan, J. Appl. Phys. **103,** 093532 (2008).

[28]M. Cazayous, and D. Malka, Appl. Phys. Lett. **91,** 071910 (2007).

[29]M. K. Singh, S. Ryu, and H. M. Jang, Phys. Rev. B **72**, 132101 (2005).

[30]D. Kothari, V. Raghavendra Reddy, A. Gupta, V. Sathe, and A. Banerjee, Appl. Phys. Lett. **91**, 202505 (2007)

[31]Z. Quan, W. Liu, H. Hu, S. Xu, B. Sebo, G. Fang, M. Li, and X. Z. Zhao, J. Appl. Phys. **104**, 084106 (2008)

[32]D. Wu, Y. Deng, C. L. Mak, K. H. Wong, A. D. Li, M. S. Zhang, and N. B. Ming, Appl. Phys. A **80,** 607 (2005).

[33]Y. Yang, L. G. Bai, K. Zhu, Y. L. Liu, S. Jiang, J. Liu, J. Chen, X. R. Xing, J. Phys.: Condens. Matter. **21**, (2009) 385901.

[34]I. Sosnowska, T. P Neumaier, and E. Steichele, J. Phys. C **15,** 4835 (1982).

[35]A. M. Kadomtsev, Y. F. Popov, A. P. Pyatakov, G. P. Vorobiev, A. K. Zvezdin, and D. Viehland, Phase Transitions **79**, 1019 (2006).

[36]M. B. Bellaki, V. Manivannan, C. Madhu, and A. Sundaresan, Mater Chem Phys. **116,** 599 (2009).

[37]K. Deepti, V. R. Reddy, A. Gupta, C. Meneghini, G. Aquilanti, J. Phys.: Condens. Matter **22,** 356001 (2010).

[38]W. H. Sung, R. C. Kang, and S. K. Chul, J Supercond Nov Magn. **24,** 635 (2011).

[39]M. A. Ahmed, and S. I. El-Dek, Mater. Lett. **60,** 1437 (2006).

[40]M. Eibschutz, S. Shtrikman, and D. Treves, Phys. Rev. B **156,** 2 (1967).

[41]B. Tiwari, and R. N. P. Choudhary, J. Alloys Compd. **493,** 1 (2010).

[42]D. Mekam, S. Kacimi, M. Djermouni, M. Azzouz, A. Zaoui, Results in Physics **2** 156 (2012).

[43]S. Sen, R. N. P. Choudhary, Mat chem phys. **87**, (2004) 256–263.

[44] A. Laha, S. B. Krupanidhi, Mater. Sci. Eng. B **98** 204-212 (2003).

[45]J. Liu, C. G. Duan,, W. G. Yin, W. N. Mei, R. W. Smith, and J. R. Hardy, Phys. Rev. B **70,** 144106 (2004).

[46]A. R. West, D. C. Sinclair, and N. Hirose, J. Electroceram. **1,** 65 (1997).

[47]J. R. Macdonald, Impedance Spectroscopy, (John Wiley and Sons, New York, 1987) Chapter 4.

[48]M. Sural, and A. Ghosh, J. Phys.: Condens. Matter. **10,** 10577 (1998).

[49]A. K. Jonscher, Nature **267,** 673 (1977).

[50]A. Ghosh, Phys. Rev. B **47,** 23 (1993).

[51]G. E. Pike, Phys. Rev. B **6,** 4 (1972).